esac

NIRSpec Performance Report
NPR-2013-008 / ESA-JWST-RP-19657
Authors: C. Alves de Oliveira & G. De Marchi
Date of Issue: 24 May 2013
Version: 1

European Space
Astronomy Centre
P.O. Box 78
28691 Villanueva de la Cañada
Madrid
Spain
Tel. (34) 91 8131 100
Fax (34) 91 8131 139
www.esa.int

Calibration of the GWA position sensors – Part II

ABSTRACT

This report presents a new method to calibrate the position sensors of the NIRSpec grating wheel assembly (GWA) based on spectral analysis. Several tests were devised and implemented to determine its accuracy and quantify the effects of the uncertainty in the mechanical angular reproducibility of the GWA on the wavelength calibration. The calibration of the sensors is achieved by applying this new method to over a thousand spectra extracted from the data acquired in the second calibration campaign of the flight model. It is shown that, using the sensors telemetry data, the position of a spectrum on the detector can be predicted with an accuracy greater than that required for wavelength calibration.

1 INTRODUCTION

The NIRSpec Grating Wheel Assembly (GWA) is a cryogenic wheel mechanism that can be configured to position one of its optical elements into the beam path. It is equipped with six dispersion gratings (R ~ 1000 and R ~ 3000), a prism (R ~ 100), and a mirror for target acquisition. The rotational degree of freedom of the wheel is given by a ball bearing controlled by two mechanisms: a cryogenic torque motor used as actuator, and a spring operated ratchet to achieve accurate positioning. Additional electrical components include temperature and tip/tilt sensors, and a harness that connects them to the unit (Weidlich et al. 2008).

The GWA components are located in the pupil plane of the instrument, dispersing or reflecting the beam to the camera that focuses it onto the focal plane assembly. The optical alignment of the wheel at instrument level, and that of the optical elements with respect to each other, ensures maximum throughput and minimum stray-light and minimizes any image displacement in the instrument's field of view. However, the ball bearing mechanism limits the mechanical angular reproducibility of the wheel, resulting in a boresight shift of the selected disperser when the wheel is moved, impacting the position of the dispersed or reflected beam on the focal plane. NIRSpec's stringent operation mode requires the

angular position of the GWA mechanism to be known to a higher accuracy, i.e., approximately 5 and 10 times better than the typical reproducibility for spectral calibration and target acquisition, respectively (RD01). To overcome the limitations on the accuracy to which the grating wheel can be positioned, two position sensors are used to measure the tip/tilt pointing error of each selected GWA optical element (De Marchi et al. 2012).

In this report, we present the method devised to calibrate the GWA position sensors by:

(1) *deriving the relation between the sensor voltage reading and the angular positional deviation of the grating wheel measured from the shift of the beam on the focal plane,*

(2) *demonstrating that this relation can be calibrated to a higher precision than required for NIRSpec optimal science operations.*

The method relies on spectral cross-correlation, and therefore it is applicable to all the dispersers. The calibration of the mirror is presented in De Marchi & Giardino (2013). The structure of this report is as follows. In Section 2 we describe the data used and their analysis, while Section 3 is devoted to explaining the method. The results of the sensor's calibration are described in Section 4, while summary and conclusions follow in Section 5.

2 DATA REDUCTION

In this section we briefly present the data selected for analysis from cycle 1 of the second NIRSpec flight model calibration campaign (hereafter FM2) that took place at IAGB, Ottobrunn, Germany from December 2012 to February 2013 (Gnata 2013). The data processing, including the extraction of the spectra, are also described.

2.1 The dataset

The data selected for analysis comprise exposures taken during the 'MOS-COMBO' procedure. There are a total of 41 repetitions of the same test sequence that cycles through different instrumental configurations, the only difference being the configuration of the micro-shutter array. During these tests, the temperature of the bench recorded was constant around 39.58 K.

For each disperser, we analyse spectra from four long slits (S200A1, S200A2, S400A1, S200B1) for a given combination of lamp source and filter, monitoring the position on the dispersion axis of prominent spectral features (emission or absorption lines). For a given instrumental configuration, any recorded shift of a line arises from the positional uncertainty of the grating wheel. Table 1 summarizes the exposures and wavelength range analysed for each disperser of the GWA. For the high-resolution gratings, the spectra taken with the long slit S200B1 were not used since they were only partly seen on the detector.

2.2 Data processing

The raw data was reduced with the pre-processing pipeline (Birkmann 2011) that performs a ramp fitting while applying bias subtraction, reference pixel subtraction,

linearity correction, and dark current subtraction. The final output is a count-rate image file, with the associated variance and quality flags for every pixel.

Each of the exposures selected for the analysis was then further processed with the NIRSpec IPS Pipeline Software (Dorner 2013). The pipeline provides a fully automated spectral extraction process. By polling the telemetry information from each exposure to identify the instrument configuration, it uses the instrument model to make an automated decision of the optimal parameters to extract and calibrate each spectrum. The pipeline uses a preliminary version of the NIRSpec model as calibrated at the present date, which already includes a first solution of the GWA tilt correction. We have followed standard steps for the spectral reduction, applying the flatfield correction (using CAA spectra), rectification of the 2D spectrum to regular coordinates, background subtraction, and finally the computation of a 1D spectrum.

One of the corrections implemented by the pipeline is the position of the grating wheel at each configuration, precisely the parameter for which we want to improve the calibration. Therefore, when extracting the spectra we disabled this correction. This means that the spectra are extracted assuming that for each configuration the respective disperser is exactly at the nominal position. Furthermore, we extracted each spectrum as a function of exiting angle from the disperser. This allows us to work in a domain that is easily related to the grating wheel coordinate system (as opposed, for example, to the wavelength scale). The extraction pipeline is written in Python and is highly modular. It is therefore possible to combine the relevant methods to achieve this tailored extraction. For this study, we extracted 1025 spectra in the manner described above.

3 METHOD TO MEASURE SPECTRAL SHIFTS

The methodology employed to characterize the effect of the uncertainty in the mechanical angular reproducibility of the GWA is presented.

3.1 Cross-spectral analysis

The uncertainty in the angular position of the grating wheel implies that, when the wheel is moved in between two exposures taken with the same configuration of illuminating source and dispersive element, the two otherwise identical spectra will be dispersed onto different positions on the focal plane. If this information (the exact position of the grating wheel) is not included in the instrument model used to extract the spectra, the expected nominal position on the detector of a spectrum taken with that configuration will be assumed. This results in two identical spectra that are offset along the dispersion axis. By measuring this shift, we can derive the real angular difference of the grating wheel position between the two exposures.

Table 1 – Data

Disperser	Lamp	Spectral range (μm)		Number of spectra	NIDs
G140M	REF (CAA)	1.4	1.5	164	9594,9645,9921,9972,10056,10220,10271,10322,10373,10436,10487,10538,10593,10644,10695,10759,10810,10861,10912,10963,11014,11065,11116,11180,11231,11282,11333,11384,11435,11486,11537,11601,11652,11703,11754,11805,11856,11907,11958,12022,12073
G140H	REF (CAA)	1.5	1.55	123	9571,9622,9898,9949,10033,10197,10248,10299,10350,10413,10464,10515,10570,10621,10672,10736,10787,10838,10889,10940,10991,11042,11093,11157,11208,11259,11310,11361,11412,11463,11514,11578,11629,11680,11731,11782,11833,11884,11935,11999,12050
G235M	REF (CAA)	2.86	3.0	164	9600,9651,9927,9978,10062,10226,10277,10328,10379,10442,10493,10544,10599,10650,10701,10765,10816,10867,10918,10969,11020,11071,11122,11186,11237,11288,11339,11390,11441,11492,11543,11607,11658,11709,11760,11811,11862,11913,11964,12028,12079
G235H	LINE2 (CAA)	2.3	2.7	123	9579,9630,9906,9957,10041,10205,10256,10307,10358,10421,10472,10523,10578,10629,10680,10744,10795,10846,10897,10948,10999,11050,11101,11165,11216,11267,11318,11369,11420,11471,11522,11586,11637,11688,11739,11790,11841,11892,11943,12007,12058
G395H	REF (CAA)	4.5	4.65	123	9586,9637,9913,9964,10048,10212,10263,10314,10365,10428,10479,10530,10585,10636,10687,10751,10802,10853,10904,10955,11006,11057,11108,11172,11223,11274,11325,11376,11427,11478,11529,11593,11644,11695,11746,11797,11848,11899,11950,12014,12065
G395M	REF (CAA)	4.25	4.65	164	9609,9660,9936,9987,10071,10235,10286,10337,10388,10451,10502,10553,10608,10659,10710,10774,10825,10876,10927,10978,11029,11080,11131,11195,11246,11297,11348,11399,11450,11501,11552,11616,11667,11718,11769,11820,11871,11922,11973,12037,12088
Prism	LINE4 (CAA)	2.1	3.3	164	9611,9662,9938,9989,10073,10237,10288,10339,10390,10453,10504,10555,10610,10661,10712,10776,10827,10878,10929,10980,11031,11082,11133,11197,11248,11299,11350,11401,11452,11503,11554,11618,11669,11720,11771,11822,11873,11924,11975,12039,12090

The method developed to derive these spectral offsets relies on the cross-correlation function, a measure of the correlation between two spectra, to estimate the most likely spectral-lag between the two. For each disperser, we have restricted the analysis to a range containing well-defined spectral features (absorption or emission lines), and a high signal-to-noise (these are given in Table 1). Figure 1 shows an example of applying the method to two spectra taken with the G140H grism and the CAA/REF lamp. The top panel (a) shows the complete spectrum of the exposure used as reference, where the flux is plotted as a function of exit angle from the dispersive element. Highlighted in green is the region used for the correlation, and in blue the small region used to derive the spectrum continuum, which is subtracted prior to the analysis. Panel (b) compares the same spectrum (blue line, NID 10464) with a spectrum taken with the same instrumental set-up after the grating wheel has been moved (red line, NID 11578). The offset of the absorption lines along the dispersed direction is evident. Panel (c) is the resulting cross-correlation for each spectral-

lag (black points), with the points around the peak fitted with a Gaussian (red line) used to derive the centroid (green line). Panels (d) and (e) show the reference spectrum (blue line, NID 10464) with the second spectrum (red line, NID 11578) overplotted after the correction has been applied, and the residuals between the two, respectively.

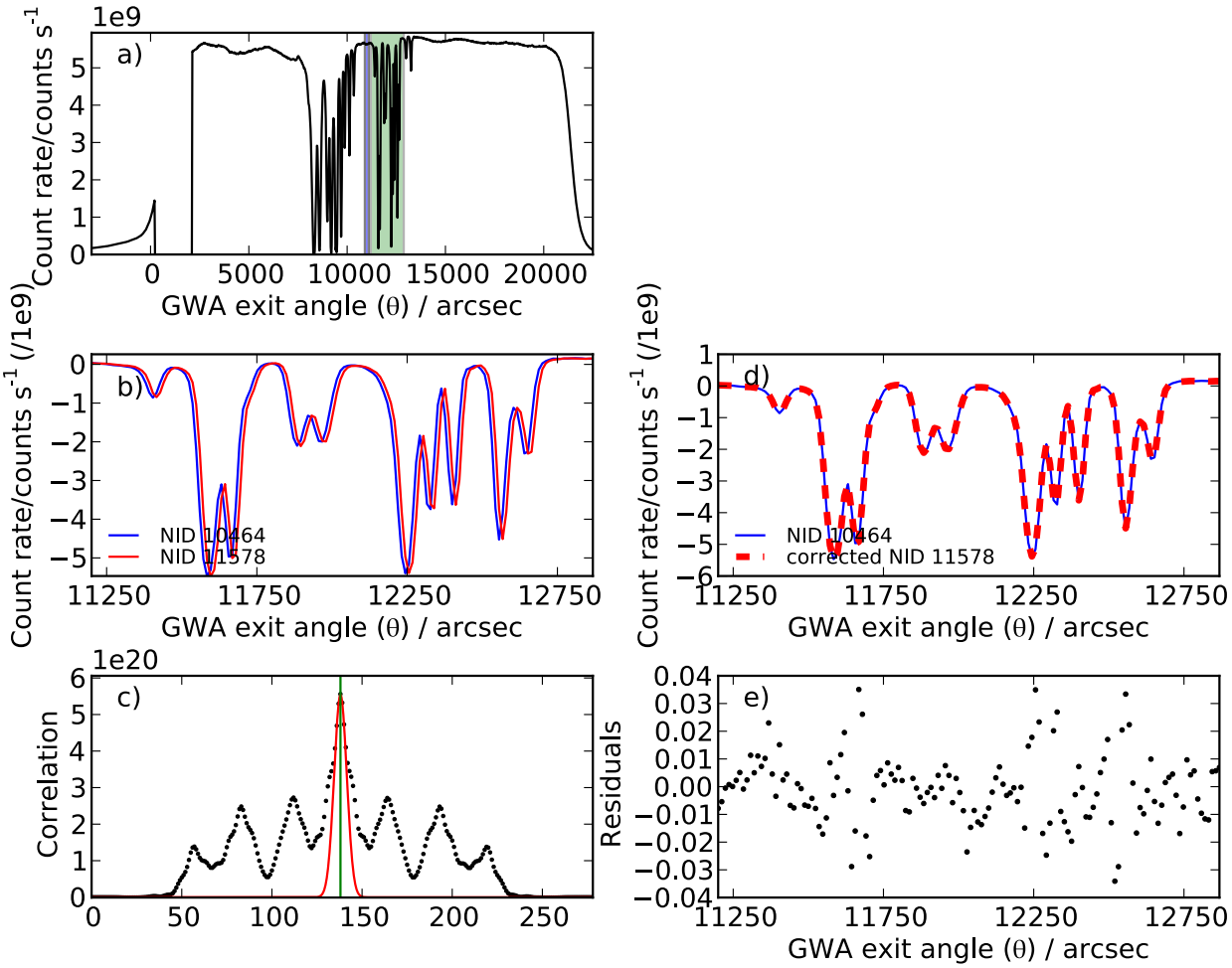

Figure 1 – Example of applying the cross-spectral analysis to correct the offset in the dispersion direction between two spectra taking at different times, but with the same instrumental set-up.

3.2 Estimation of the uncertainties

To estimate the uncertainties of the cross-correlation analysis, we use a Monte-Carlo simulation to propagate uncertainties in the input spectra into the measured peak of the cross-correlation. For each of two given spectra taken with the same instrumental set-up, we associate an uncertainty value to each spectral element drawn from a randomly generated normal distribution, which is multiplied by the photon noise and added to the flux. The cross-correlation function is computed and its peak is derived using a Gaussian fit. The same analysis is repeated for 10 000 realizations of randomly generated values. An example of the shift distribution found for two exposures is shown in Fig. 2. The mean value and standard deviation of this distribution are the final shift and its 1-σ error.

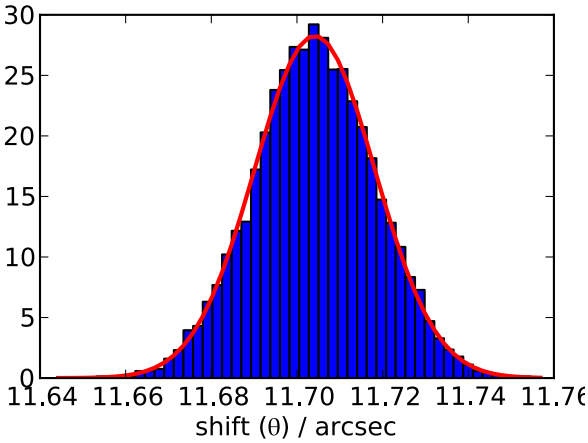

Figure 2 – Distribution of shifts derived using the Monte-Carlo method. The resulting shift measurement for this combination of spectra (same as Fig. 1) is 11.704 + 0.014 arcsec.

3.3 Testing the method's precision

We tested the method's precision limitation by comparing a spectrum with itself, and progressively injecting an offset in arcsec, and calculating the shift. The results are shown in Fig. 3. The precision reached with the method is of order 0.0033 arcsec. This precision is much smaller than the typical shifts that we are measuring.

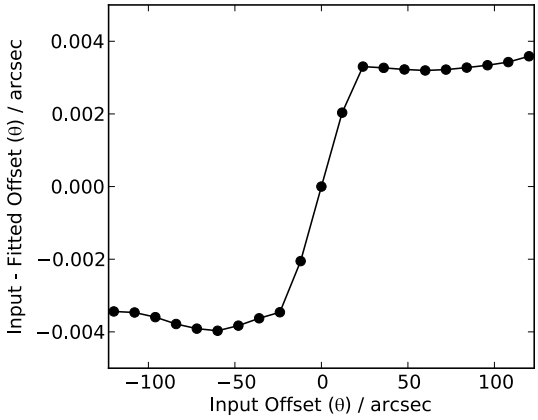

Figure 3 – Difference between an artificially added shift and the shift derived using the cross-correlation algorithm.

3.4 Uncertainty from sensor reading

To estimate the impact of the error on the calibration of the sensor reading in the extraction, we ran a Monte-Carlo simulation to propagate uncertainties in the angle of the grating wheel into the shift between two extracted spectra (measured with the cross-correlation method presented in Section 3.1). For each exposure, we generated 10 000 random values of the grating wheel positional angle that were normally distributed with mean of zero and a standard deviation of 0.2 arcsec (corresponding to the angular resolution allowed by the position sensors on the wheel). For each exposure, we extracted a spectrum using one of the randomly polled angle values, and applied the cross-correlation

method to derive the angular shift, repeating the process 10 000 times. The results are shown in Fig. 4. This error will be added to the error budget in the calibration of the sensors.

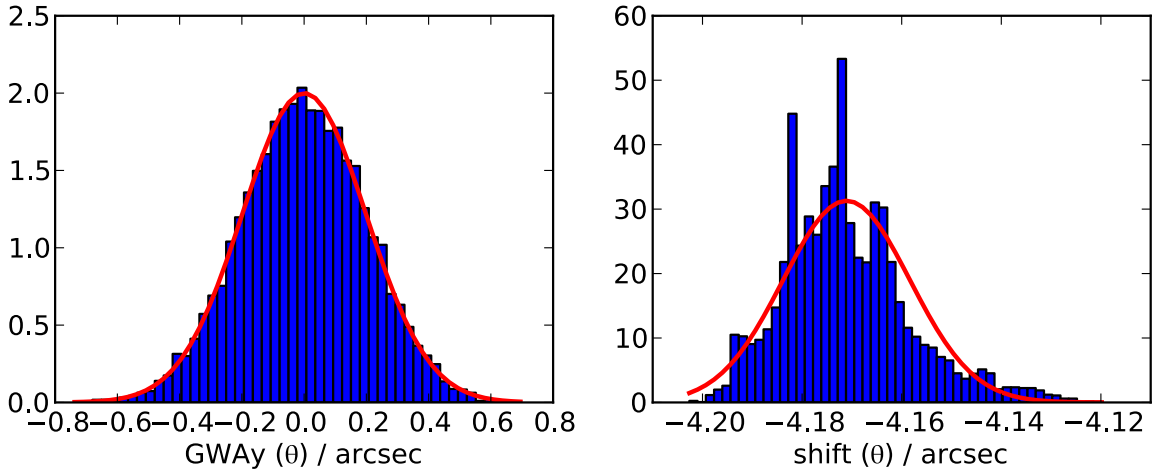

Figure 4 – Left panel: Randomly generated angles of the grating wheel position. Right panel: Distribution of the measured shifts derived using the Monte-Carlo method (NID 10464 and NID 10350, G140H, S200A1).

4 RESULTS OF THE SENSORS CALIBRATION

For each instrumental set-up, we compare the telemetry from the sensor voltage reading to the angular shift of the dispersed beam on the focal plane derived from the cross-spectral analysis. Different methods have been implemented to read the voltage of GWA sensors, resulting in three different values that are included in the telemetry stored in the header of an exposure (GWA_XP_V, GWA_PXAV, GWA_XTIL), as described in De Marchi (2012). The results are presented in Fig. 5 and Tables 2, 3 and 4, showing the linear fit for the long slits (S200A1, S200A2, S400A, and S200B), and the fit to the residuals. These relations are known to change with the temperature of the optical bench (De Marchi 2012; De Marchi et al. 2012), and therefore the final values will be re-computed once the telescope is in orbit.

The rms of the residuals provides an estimate of the accuracy of the sensor calibration method presented here. For all dispersers and sensor readings, the rms is always below 0.06 pixels, meeting the allocated fraction of the wavelength calibration budget for wavelength zero-point calibration (~1/10 of a pixel, as explained in Ferruit 2005) dictated by requirement R119 of the NIRSpec System Requirements Document (Jensen 2013). The method present here cannot be applied to study the impact of the GWA mechanical reproducibility in the cross-dispersion direction. However, this topic is addressed in De Marchi & Giardino (2013), where it is shown that the shifts measured in the focal plane in the cross-dispersion direction are typical 2.5 mas or ~1/40 of a pixel, and therefore no correction is needed.

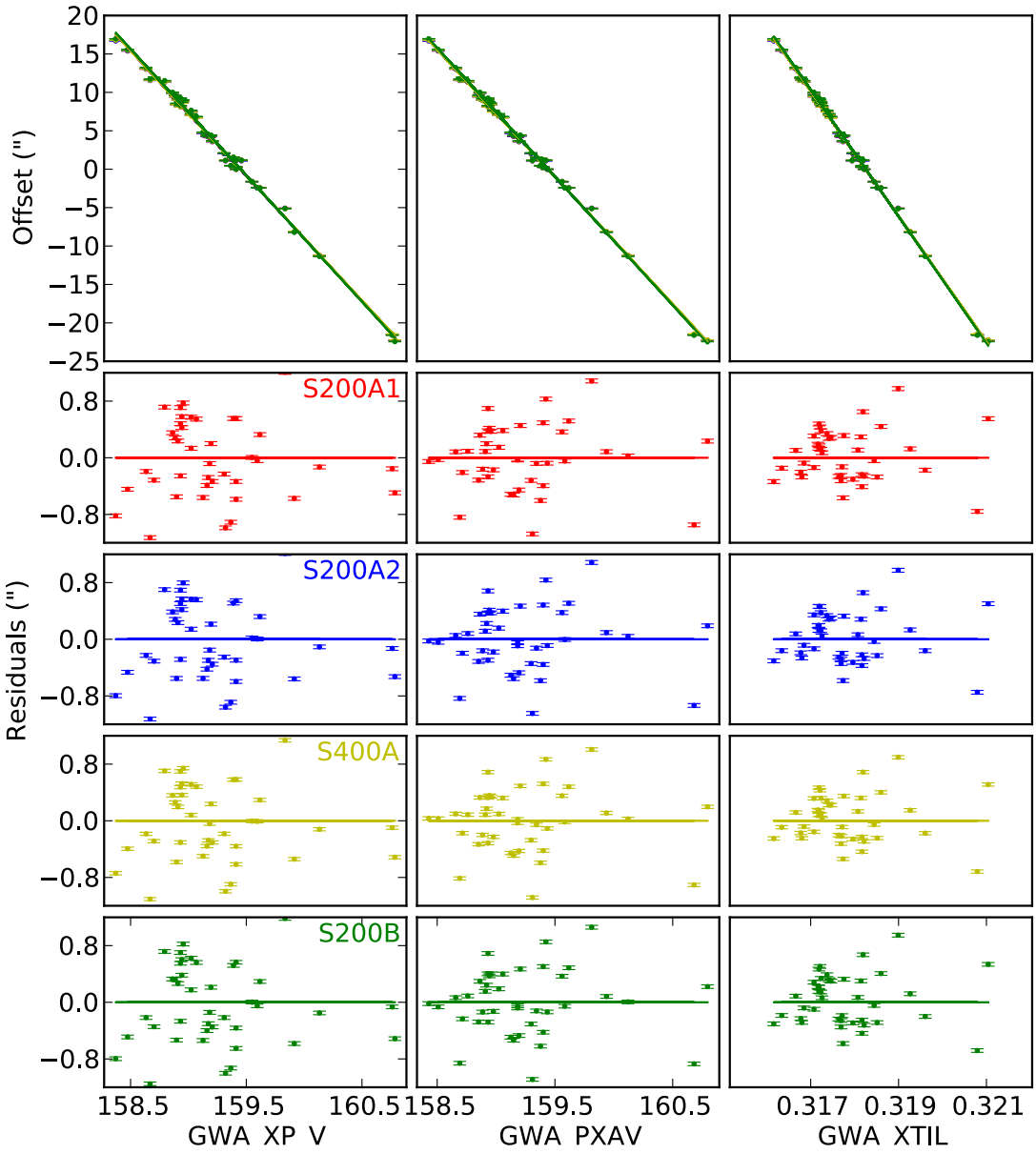

Figure 5 – Relation between measured spectral shifts and GWA position sensor telemetry (G235M).

5 CONCLUSIONS

We have presented a method based on cross-spectral analysis to calibrate position sensors of the dispersers on the grating wheel. The method is applied to over one thousand spectra collected during the second calibration campaign of the NIRSpec flight model, to derive the relative shift in the position of a spectrum on the focal plane along the dispersion direction. The calibration of the sensors is achieved by establishing the relation between the relative position sensor readings and the measured spectral shift, a proxy for the angular positional deviation of the grating wheel. For any combination of disperser and type of sensor reading, the rms of the calibration relation is found to be below 0.06 pixels. This

demonstrates that the mechanical angular position of the grating wheel can be determined with a greater precision than the minimum requirement for NIRSpec optimal science operations. Our findings show that the precision reached with the GWA calibration method presented in this report is considerably better than the ~1/10 of a pixel allocated for the wavelength zero-point in the wavelength calibration error budget and, as such, it is fully consistent with requirement R119 of the NIRSpec System Requirements Document (Jensen 2013).

Table 2 – Results for sensor reading GWA_XTIL.

GRISM	Slit	Fit to spectral shift (A+Bx)				Fit to residuals(C+Dx)		RMS of residuals	
		A	Aerr	B	Berr	C	D	(“)	(pixel)
G140M	S200A1	2724.906	54.115	-8320.326	165.299	0.00010	-0.00029	0.475	0.036
	S200A2	2728.907	54.071	-8332.504	165.164	-0.00150	0.00458	0.475	0.036
	S400A	2750.847	49.742	-8399.517	151.934	-0.00068	0.00207	0.455	0.034
	S200B	2792.674	51.469	-8527.157	157.21	-0.00050	0.00152	0.478	0.036
G140H	S200A1	3312.381	34.900	-9195.405	97.119	0.00012	-0.00034	0.472	0.036
	S200A2	3304.390	35.525	-9173.313	98.856	-0.0006	0.00166	0.475	0.036
	S400A	3306.742	33.826	-9179.776	94.122	-0.00036	0.00101	0.464	0.035
G235M	S200A1	2597.477	20.834	-8161.81	65.557	-0.00014	0.00043	0.414	0.031
	S200A2	2596.417	20.557	-8158.441	64.683	-0.00006	0.00018	0.410	0.031
	S400A	2594.610	20.053	-8152.699	63.096	0.00003	-0.00010	0.398	0.030
	S200B	2625.139	20.878	-8248.542	65.692	-0.00031	0.00096	0.417	0.032
G235H	S200A1	2931.754	46.92	-8328.473	133.147	0.00105	-0.00298	0.556	0.042
	S200A2	2949.945	55.342	-8378.884	157.06	-0.00243	0.00688	0.511	0.039
	S400A	2923.049	34.98	-8302.623	99.269	0.00003	-0.00008	0.409	0.031
G395M	S200A1	2224.312	16.482	-7914.017	58.397	-0.00008	0.00029	0.441	0.033
	S200A2	2219.389	14.823	-7896.459	52.507	-0.00002	0.00008	0.432	0.033
	S400A	2223.552	14.183	-7911.302	50.237	-0.00007	0.00026	0.414	0.031
	S200B	2250.165	14.870	-8005.803	52.670	0.00000	0.00001	0.441	0.034
G395H	S200A1	2639.358	38.539	-8278.354	120.724	-0.00068	0.00213	0.421	0.032
	S200A2	2628.605	37.953	-8244.691	118.889	-0.00099	0.00311	0.405	0.031
	S400A	2642.719	37.897	-8288.888	118.713	0.00028	-0.00089	0.41	0.031
PRISM	S200A1	2766.702	17.655	-8236.524	52.406	-0.00001	0.00004	0.542	0.042
	S200A2	2749.100	19.469	-8184.340	57.821	0.00009	-0.00026	0.577	0.044
	S400A	2764.652	19.230	-8230.224	57.089	-0.00006	0.00018	0.579	0.045
	S200B	2703.904	18.314	-8049.888	54.379	-0.00003	0.00010	0.556	0.042

Table 3 – Results for sensor reading GWA_XP_V.

GRISM	Slit	Fit to spectral shift (A+Bx)				Fit to residuals(C+Dx)		RMS of residuals	
		A	Aerr	B	Berr	C	D	(“)	(pixel)
G140M	S200A1	2750.332	74.103	-16.762	0.452	-0.01017	0.00006	0.639	0.048
	S200A2	2753.985	74.093	-16.784	0.452	0.00901	-0.00005	0.639	0.048
	S400A	2782.772	70.423	-16.959	0.429	-0.00186	0.00001	0.629	0.048
	S200B	2838.560	69.734	-17.299	0.425	-0.00499	0.00003	0.645	0.049
G140H	S200A1	3339.986	45.191	-18.506	0.251	0.00137	-0.00001	0.604	0.046
	S200A2	3331.735	45.723	-18.461	0.254	-0.00046	0.00000	0.605	0.046
	S400A	3335.060	45.144	-18.479	0.251	0.00112	-0.00001	0.612	0.047
G235M	S200A1	2595.047	28.665	-16.275	0.180	-0.00429	0.00003	0.570	0.043
	S200A2	2595.636	28.498	-16.279	0.179	0.00262	-0.00002	0.569	0.043
	S400A	2593.877	27.928	-16.268	0.175	-0.00445	0.00003	0.555	0.042
	S200B	2623.438	29.004	-16.453	0.182	0.00226	-0.00001	0.580	0.044
G235H	S200A1	2918.231	57.238	-16.546	0.324	-0.00559	0.00003	0.679	0.053
	S200A2	2990.089	76.969	-16.951	0.436	-0.02356	0.00013	0.74	0.056
	S400A	2903.323	50.29	-16.46	0.285	-0.00016	0.00000	0.596	0.045
G395M	S200A1	2193.282	20.527	-15.576	0.145	-0.00077	0.00001	0.566	0.043
	S200A2	2198.444	18.905	-15.612	0.134	-0.00023	0.00000	0.563	0.043

	S400A	2202.59	18.611	-15.641	0.132	-0.00236	0.00002	0.553	0.042
	S200B	2227.963	19.645	-15.821	0.139	-0.00159	0.00001	0.595	0.045
G395H	S200A1	2582.772	49.901	-16.168	0.312	0.00617	-0.00004	0.544	0.041
	S200A2	2571.518	49.609	-16.098	0.310	0.00303	-0.00002	0.537	0.041
	S400A	2585.552	49.603	-16.186	0.310	-0.00730	0.00005	0.542	0.041
PRISM	S200A1	2770.897	19.596	-16.464	0.116	0.00187	-0.00001	0.608	0.047
	S200A2	2749.807	23.037	-16.340	0.137	0.00295	-0.00002	0.632	0.049
	S400A	2764.920	21.567	-16.429	0.128	-0.00424	0.00003	0.627	0.048
	S200B	2705.439	20.857	-16.076	0.124	-0.00391	0.00002	0.610	0.046

Table 4 – Results for sensor reading GWA_PXAV.

GRISM	Slit	Fit to spectral shift (A+Bx)				Fit to residuals (C+Dx)		RMS of residuals	
		A	Aerr	B	Berr	C	D	(“)	(pixel)
G140M	S200A1	2731.602	66.699	-16.649	0.407	0.00509	-0.00003	0.579	0.044
	S200A2	2734.731	66.672	-16.668	0.407	-0.00385	0.00002	0.578	0.044
	S400A	2762.245	62.358	-16.835	0.380	0.00135	-0.00001	0.564	0.043
	S200B	2804.079	64.729	-17.090	0.395	0.00880	-0.00005	0.585	0.045
G140H	S200A1	3280.644	36.942	-18.178	0.205	0.00418	-0.00002	0.501	0.038
	S200A2	3271.804	37.406	-18.129	0.208	0.00153	-0.00001	0.504	0.038
	S400A	3275.989	36.083	-18.152	0.200	-0.00207	0.00001	0.501	0.038
G235M	S200A1	2642.572	23.283	-16.574	0.146	0.00026	0.00000	0.455	0.034
	S200A2	2641.937	23.096	-16.570	0.145	0.00573	-0.00004	0.453	0.034
	S400A	2639.646	22.624	-16.556	0.142	-0.00030	0.00000	0.442	0.034
	S200B	2671.112	23.133	-16.753	0.145	-0.00163	0.00001	0.454	0.035
G235H	S200A1	2923.939	45.74	-16.579	0.259	-0.00414	0.00002	0.544	0.041
	S200A2	2949.973	56.463	-16.725	0.32	0.00012	0.00000	0.516	0.039
	S400A	2909.454	36.059	-16.495	0.204	0.00284	-0.00002	0.425	0.032
G395M	S200A1	2208.515	18.937	-15.685	0.134	-0.00005	0.00000	0.509	0.039
	S200A2	2208.792	17.260	-15.687	0.122	-0.00214	0.00002	0.506	0.038
	S400A	2213.018	16.749	-15.717	0.118	0.00275	-0.00002	0.492	0.037
	S200B	2239.148	17.529	-15.902	0.124	0.00133	-0.00001	0.521	0.040
G395H	S200A1	2605.403	40.884	-16.311	0.256	0.00019	0.00000	0.446	0.034
	S200A2	2594.917	40.169	-16.245	0.251	0.00224	-0.00001	0.434	0.033
	S400A	2608.600	39.963	-16.331	0.250	-0.00769	0.00005	0.435	0.033
PRISM	S200A1	2763.568	18.329	-16.422	0.109	-0.00075	0.00000	0.579	0.044
	S200A2	2743.474	20.948	-16.303	0.124	-0.00203	0.00001	0.611	0.047
	S400A	2760.694	20.107	-16.405	0.119	0.00096	-0.00001	0.605	0.047
	S200B	2699.980	19.711	-16.045	0.117	0.00158	-0.00001	0.589	0.044

6 REFERENCES

Birkmann, S. (2011), “Description of the NIRSpec pre-processing pipeline,” NTN-2011-004 (Noordwijk: ESTEC)

Böker, T. 2012, “NIRSpec Operations Concept Document,” ESA-JWST-TN-0297, (Noordwijk: ESTEC)

De Marchi, G. 2012, “Calibration of the GWA position sensors – Part I,” NPR-2012-002 (Noordwijk: ESTEC)

De Marchi, G., Birkmann, S., Böker, T., Ferruit, P., Giardino, G., et al. 2012, “Calibrating the position of images and spectra in the NIRSpec instrument for the James Webb Space Telescope,” Proc. SPIE 8442-84423G

De Marchi, G., Giardino, G. 2013, “Calibration of the GWA position sensors – Part III – Target acquisition accuracy ,” NPR-2013-006 (Noordwijk: ESTEC)

Dorner, B. 2013, “NIRSpec IPS pipeline software description,” NIRS-MPI-TN-0012 (Heidelberg: MPIA)

Ferruit, P. 2005, “Review of the in-orbit wavelength calibration of the NIRSpec instrument,” NIRS-CRAL-TN-0001 (Lyon: CRAL)

Gnata, X. 2013, “FM calibration and verification report,” NIRS-ASD-TR-0143 (Ottobrunn: EADS)

Jensen, P. 2013, “Near-Infrared Spectrograph System Requirements Document,” ESA-JWST-RQ-322 (Noordwijk: ESTEC)

Weidlich, K., Fischer, M., Ellenrieder, M.M., Gross, T., Salvignol, J.C., Barho, R., Neugebauer, C., Königsreiter, G., Trunz, M., Müller, F., Krause, O. 2008, "High-precision cryogenic wheel mechanisms for the JWST NIRSpec instrument," Proc. SPIE 7018, 64